J|A|C|S
ARTICLES
Published on Web 06/22/2004

Single-Molecule Magnets of Ferrous Cubes: Structurally Controlled Magnetic Anisotropy

Hiroki Oshio,*,† Norihisa Hoshino,‡ Tasuku Ito,‡ and Motohiro Nakano§

Contribution from the Department of Chemistry, University of Tsukuba, Tennodai 1-1-1, Tsukuba 305-8571, Japan; Department of Chemistry, Graduate School of Science, Tohoku University, Sendai 980-8578, Japan; and Department of Molecular Chemistry, Graduate School of Engineering, Osaka University, Toyonaka, Osaka 560-0043, Japan

Received March 10, 2004; E-mail: oshio@chem.tsukuba.ac.jp

Abstract: Tetranuclear Fe^{II} cubic complexes were synthesized with Schiff base ligands bridging the Fe^{II} centers. X-ray structural analyses of six ferrous cubes, $[Fe_4(sap)_4(MeOH)_4]\cdot 2H_2O$ (**1**), $[Fe_4(5\text{-Br-sap})_4(MeOH)_4]$ (**2**), $[Fe_4(3\text{-MeO-sap})_4(MeOH)_4]\cdot 2MeOH$ (**3**), $[Fe_4(sae)_4(MeOH)_4]$ (**4**), $[Fe_4(5\text{-Br-sae})_4(MeOH)_4]\cdot MeOH$ (**5**), and $[Fe_4(3,5\text{-}Cl_2\text{-sae})_4(MeOH)_4]$ (**6**) (R-sap and R-sae were prepared by condensation of salicylaldehyde derivatives with aminopropyl alcohol and aminoethyl alcohol, respectively) were performed, and their magnetic properties were studied. In **1**−**6**, the alkoxo groups of the Schiff base ligands bridge four Fe^{II} ions in a μ_3-mode forming $[Fe_4O_4]$ cubic cores. The Fe^{II} ions in the cubes have tetragonally elongated octahedral coordination geometries, and the equatorial coordination bond lengths in **4**−**6** are shorter than those in **1**−**3**. Dc magnetic susceptibility measurements for **1**−**6** revealed that intramolecular ferromagnetic interactions are operative to lead an $S = 8$ spin ground state. Analyses of the magnetization data at 1.8 K gave the axial zero-field splitting parameters (D) of +0.81, +0.80, +1.15, −0.64, −0.66, and −0.67 cm^{-1} for **1**−**6**, respectively. Ac magnetic susceptibility measurements for **4**−**6** showed both frequency dependent in- and out-of-phase signals, while **1**−**3** did not show out-of-phase signals down to 1.8 K, meaning **4**−**6** are single-molecule magnets (SMMs). The energy barriers to flip the spin between up- and down-spin were estimated to 28.4, 30.5, and 26.2 K, respectively, for **4**−**6**. The bridging ligands R-sap^{2-} in **1**−**3** and R-sae^{2-} in **4**−**6** form six- and five-membered chelate rings, respectively, which cause different steric strain and Jahn−Teller distortions at Fe^{II} centers. The sign of the D value was discussed by using angular overlap model (AOM) calculations for irons with different coordination geometry.

Introduction

High-spin molecules with an easy axis type of anisotropy have a double minimum potential in the reverse direction of the magnetic moment, and they show slow magnetic relaxation in respect to spin flipping along the magnetic anisotropy axis. At very low temperatures the spin does not thermally flip but flips via quantum processes. Molecules having such superparamagnetic behavior are called single-molecule magnets (SMMs).[1] SMMs have attracted an intense research interest due to their characteristic quantum behavior and possible application to very small memory devices. A SMM was first reported for $[Mn_{12}O_{12}(O_2CMe)_{16}(H_2O)_4]$ ([Mn12]),[2] and several analogues of [Mn12][3] and $[Fe_8O_2(OH)_{12}(tacn)_6]^{8+}$ (tacn = 1,4,7-triazacyclononane)[4] have been extensively studied. Sophisticated techniques such as high-frequency EPR (HF-EPR) and solid-state NMR spectroscopies have been used to explore the magnetic structures and quantum phenomena in SMMs.[5] While a number of SMMs containing manganese,[6] iron,[7] nickel,[8] and cobalt[9] ions have been reported, [Mn12] is still the highest blocking temperature SMM.

For cluster molecules to be classified as SMMs, they must have large uniaxial magnetic anisotropy of easy axis type and large ground state spin multiplicity. In mixed-metal or mixed-valence cluster molecules, antiferromagnetic interactions be-

† University of Tsukuba.
‡ Tohoku University.
§ Osaka University.

(1) (a) Friedman, J. R.; Sarachik, M. P.; Tejada, J.; Ziolo, R. *Phys. Rev. Lett.* **1996**, *76* (20), 3830. (b) Thomas, L.; Lionti, L.; Ballou, R.; Gatteschi, D.; Sessoli, R.; Barbara, B. *Nature* **1996**, *383*, 145. (c) Tejada, J.; Ziolo, R. F.; Zhang, X. X. *Chem. Mater.* **1996**, *8*, 1784. (d) Aubin, S. M.; Gilley, N. R.; Pardi, L.; Krzystek, J.; Wemple, M. W.; Brunel, L. C.; Marple, M. B.; Christou, G.; Hendrickson, D. N. *J. Am. Chem. Soc.* **1998**, *120*, 4991. (e) Ruiz, D.; Sun, Z.; Albela, B.; Folting, K.; Christou, G.; Hendrickson, D. N. *Angew. Chem., Int. Ed.* **1998**, 300.

(2) (a) Sessoli, R.; Gatteschi, D.; Caneschi, A.; Novak, M. A. Nature, **1993**, *115*, 1804. (b) Sessoli, R.; Ysai, H.-L.; Schake, A. R.; Wang, S.; Vincent, J. B.; Folting, K.; Gatteschi, D.; Christou, G.; Hendrickson, D. N. *J. Am. Chem. Soc.* **1993**, *115*, 1804.

(3) (a) Caneschi, A.; Gatteschi, D.; Sessoli, R.; Barra, A. L.; Brunel, L. C.; Guillot, M. *J. Am. Chem. Soc.* **1991**, *113*, 5873. (b) Friedman, J. R.; Sarachik, M. P.; Tejada, J.; Maciejewski, J.; Ziolo, R. *J. Appl. Phys.* **1996**, *79*, 6031. (c) Eppley, H. J.; Tsai, H.-L.; De Vries, N.; Folting, K.; Christou, G.; Hendrickson, D. N. *J. Am. Chem. Soc.* **1995**, *117*, 301. (d) Boskovic, C.; Pink, M.; Huffman, J. C.; Hendrickson, D. N.; Christou, G. *J. Am. Chem. Soc.* **2001**, *123*, 9914.

(4) (a) Gatteschi, D.; Sessoli, R.; Cornia, A. *Chem. Comm.* **2000**, 725. (b) Barra, A. L.; Debrunner, P.; Gatteschi, D.; Schulz, C. E.; Sessoli, R. *Europhys. Lett.* **1996**, *35*, 133. (c) Pontilon, Y.; Caneschi, A.; Gatteschi, D.; Sessoli, R.; Ressouche, E.; Schweizer, J.; Lelievre-Vera, E. *J. Am. Chem. Soc.* **1999**, *121*, 5342.

(5) (a) Aubin, S. M. J.; Dilley, N. R.; Pardi, L.; Kryzystek, J.; Wemple, M. W.; Maple, M. B.; Brunel, L.-C.; Christou, G.; Hendrickson, D. N. *J. Am. Chem. Soc.* **1998**, *120*, 4991. (b) Barra, A. L.; Gatteschi, D.; Sessoli, R. *Chem.—Eur. J.* **2000**, *6*, 1608. (c) Cornia, A.; Gatteschi, D.; Sessoli, R. *Coord. Chem. Rev.* **2001**, *219*−*221*, 573.

tween metal centers usually lead to a ferrimagnetic high-spin ground state, and this strategy has been used often to prepare SMMs. However, in homo-metal systems, ferromagnetic interactions need to have a high-spin ground state. Paramagnetic metal ions in homo-metal cluster molecules are subject to magnetic interactions via superexchange and/or spin polarization mechanisms, among which the superexchange mechanism is predominant in metal complexes bridged by single anions. The isotropic superexchange interaction is expressed by the spin Hamiltonian, $H = -2\Sigma J_{ij} S_i \cdot S_j$, where J is the exchange coupling constant. The superexchange mechanism, first proposed by Anderson, Goodenough, and Kanamori,[10] predicts the sign of the J values. When two homo-metal ions are bridged by an anion with a bridging angle of 180°, strong antiferromagnetic interactions ($J < 0$) occur. There are two ways to have ferromagnetic interactions. When different metal ions with orthogonal magnetic orbitals are bridged with a bond angle of 180°, ferromagnetic interactions occur, and if two homo-metal ions are bridged with a bond angle of 90°, the magnetic orbitals become orthogonal giving rise to a high-spin ground state.

Metal cubes, which have four metal ions and four anions are alternately aligned in the cube, often have a high-spin ground state because the magnetic orbitals of the metal ions are accidentally orthogonal. Hydroxo-, alkoxo-, azido-, and iminato-bridged metal cubes have been reported,[11] and sulfido-bridged iron cubes have been extensively studied as a model of iron−sulfur proteins.[12] Ni^{II} cubes with an $S = 4$ spin ground state have been shown to be SMMs with exchange biased quantum spin tunneling phenomena.[13] SMMs are also required to possess magnetic anisotropy in cluster molecules, which is still difficult to control. There must be some rules to determine the sign of the D value, which is related to Jahn−Teller (JT) distortion, and a simple ligand field approach gives some clues about control.[14] Ferrous cubes are good candidates for being SMMs because they can have high-spin ground states, and the magnetic anisotropy of Fe^{II} ions can be controlled by changing coordination geometries of the Fe^{II} ions. We report herein the structures and magnetic properties of ferrous cubes with two types of bridging Schiff base ligands (H_2R-sap and H_2R-sae), which cause different degrees of JT distortion. A part of this work was published in the communication.[15]

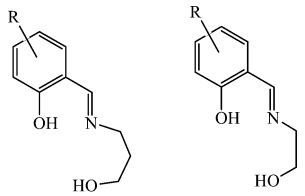

H_2R-sap H_2R-sae

Results

Descriptions of Structures. ORTEP diagrams of compounds **1**−**6** are shown in Figure 1, and selected bond lengths are summarized in Tables 1 and 2. Complexes **1**, **2**, and **6** crystallized in the tetragonal space group $I4_1/a$, and complexes **3**, **4**, and **5** crystallized in the triclinic space group $P\bar{1}$.

Complexes **1**−**6** have tetranculear cubane core structures, in which four Fe^{II} ions are bridged by μ_3-alkoxo groups, giving an approximately cubic array of alternating iron and oxygen atoms. In **1**, **2**, and **6**, the asymmetric unit contains a quarter of the complex molecule, and they have a crystallographic $\bar{4}$ axis which passes through the middle of Fe1···Fe4 and Fe2···Fe3 vectors, while the cores of **3**−**5** have a pseudo $\bar{4}$ axis. The six coordination sites of the Fe^{II} ions are occupied by five oxygen atoms and one nitrogen atom from a chelating Schiff base ligand and methanol molecules, and the point group symmetry is D_{2d}. The Fe^{II} ions have an axially elongated coordination geometry with the axial sites occupied by oxygen atoms from methanol and a bridging alkoxide. The elongated axis (axial axis) of the each Fe^{II} ion lies perpendicular to the molecular S_4 axis, and two sets of elongated axes, one set lying on the upper face and the lower on the other face of the cube, are perpendicular to each other. Disregarding the difference in Schiff base ligands, the complexes are classified into two groups, **1**−**3** and **4**−**6**, based on the coordination bond lengths of the equatorial ligands. In **1**−**3**, the average coordination bond lengths involving the axial atoms are 2.230(2), 2.261(4), and 2.240(6) Å, and the equatorial coordination bond lengths are in the ranges 2.0290(16)−2.1616(15), 2.036(3)−2.159(3), and 1.991(5)−2.134(4)

(6) (a) Soler, M.; Wernsdofer, W.; Abboud, K. A.; Huffman, J. C.; Davidson, E. R.; Hendrickson, D. N.; Christou, G. *J. Am. Chem. Soc.* **2003**, *125*, 3576. (b) Boskovic, C.; Brechin, E. K.; Streib, W. E.; Folting, K.; Bollinger, J. C.; Hendrickson, D. N.; Christou, G. *J. Am. Chem. Soc.* **2003**, *124*, 3725. (c) Brechim, E. K.; Boskovic, C.; Wernsdofer, W.; Yoo, J.; Yamaguchi, A.; Sanudo, E. C.; Concolino, T. R.; Rheingold, A. L.; Ishimoto, H.; Hendrickson, D. N.; Christou, G. *J. Am. Chem. Soc.* **2002**, *124*, 9710. (d) Wernsdorfer, W.; Aliaga-Alcalde, N.; Hendrickson, D. N.; Christou, G. *Nature* **2002**, *416*, 406. (e) Aromi, G.; Bhaduri, S.; Artus, P.; Folting, K.: Christou, G. *Inorg. Chem.* **2002**, *41*, 805. (f) Boskovic, C.; Brechin, E. K.; Streib, W. E.; Folting, K.; Bollinger, J. C.; Hendrickson, D. N.; Christou, G. *J. Am. Chem. Soc.* **2002**, *124*, 3725. (g) Price, J. P.; Batten, S. R.; Moubaraki, B.; Murray, K. S. *Chem. Commun.* **2002**, 762. (h) Brechin, E. K.; Boskovic, C.; Wernsdorfer, W.; Yoo, J.; Yamaguchi, A.; Sañudo, E. C.; Concolino, T. R.; Rheingold, A. L.; Ishimoto, H.; Hendrickson, D. N.; Christou, G. *J. Am. Chem. Soc.* **2002**, *124*, 9710. (i) Brockman, J. T.; Huffman, J. C.; Christou, G. *Angew. Chem., Int. Ed.* **2002**, *41*, 2506. (j) Soler, M.; Artus, P.; Folting, K.; Huffman, J. C.; Hendrickson, D. N.; Christou, G. *Inorg. Chem.* **2001**, *40*, 4902. (k) Aliaga-Alcalde, N.; Folting, K.; Hendrickson, D. N.; Christou, G. *Polyhedron* **2001**, *20*, 1273. (l) Andres, H.; Basler, R.; Gudel, H.-U.; Aromi, G.; Christou, G.; Buttner, H.; Ruffle, B. *J. Am. Chem. Soc.* **2000**, *122*, 12469. (m) Artus, P.; Boskovic, C.; Yoo, J.; Streib, W. E.; Brunel, L.-C.; Hendrickson, D. N.; Christou, G. *Inorg. Chem.* **2001**, *40*, 4199. (n) Soler, M.; Rumberger, E.; Folting, K.; Hendrickson, D. N.; Christou, G. *Polyhedron* **2001**, *20*, 1365. (o) Aubin, S. M. J.; Sun, Z.; Pardi, L.; Krzystek, J.; Folting, K.; Brunel, L.-C.; Rheingold, A. L.; Christou, G.; Hendrickson, D. N. *Inorg. Chem.* **1999**, *38*, 5329. (p) Aubin, S. M. J.; Wemple, M. W.; Adams, D. M.; Tsai, H.-L.; Christou, G.; Hendrickson, D. N. *J. Am. Chem. Soc.* **1996**, *118*, 7746. (q) Eppley, H. J.; Tsai, H.-L.; Vries, N.; Folting, K.; Christou, G.; Hendrickson, D. N. *J. Am. Chem. Soc.* **1995**, *117*, 301.

(7) (a) Sangregorio, C.; Ohm, T.; Paulsen, C.; Sessoli, R.; Gatteschi, D. *Phys. Rev. Lett.* **1997**, *78*, 4645. (b) Oshio, H.; Hoshino, N.; Ito, T. *J. Am. Chem. Soc.* **2000**, *122*, 12602. (c) Barra, A. L.; Caneschi, A.; Cornia, A.; Fabrizi de Biani, F.; Gatteschi, D.; Sangregorio, C.; Sessoli, R.; Sorace, L. *J. Am. Chem. Soc.* **1999**, *121*, 5302.

(8) Cadiou, C.; Murrie, M.; Paulsen, C.; Villar, V.; Wernsdorfer, W.; Winpenny, R. E. P. *Chem. Commun.* **2001**, 2666.

(9) Yang, E.-C.; Hendrickson, D. N.; Wernsdorfer, W.; Nakano, M.; Zakharov, L. N.; Sommer, R. D.; Rheingold, A. L.; Ledezma-Gairaud, M.; Christou G. *J. Appl. Phys.* **2002**, *91*, 7382.

(10) (a) Anderson, P. W. *Phys. Rev.* **1959**, *115*, 2. (b) Kanamori, J. *J. Phys. Chem. Solids* **1959**, *10*, 87 1959. (c) Goodenough, J. B. *J. Phys. Chem. Solids* **1958**, *1*, 287.

(11) (a) Halcrow, M. A.; Huffman, J. C.; Christou, G. *Angew. Chem., Int. Ed. Engl.* **1995**, *34*, 889. (b) Halcrow, M. A.; Sun, J.-S.; Huffman, J. C.; Christou, G. *Inorg. Chem.* **1995**, *34*, 4167. (c) Mai, H.-J.; Köcker, R. M.; Wocadlo, S.; Massa, W.; Dehnicke, K.; *Angew. Chem., Int. Ed. Engl.* **1995**, *34*, 1235. (d) Mertz, L.; Haase, W. *J. Chem. Soc., Dalton Trans.* **1978**, 1594. (e) Schawabe, L.; Haase, W.; *J. Chem. Soc., Dalton Trans.* **1985**, 1909. (f) Hall, J. W.; Estes, W. E. D.; Scaringe, R. P.; Williams, W. E. *Inorg. Chem.* **1977**, *16*, 1572. (g) Sleten, J.; Sorensen, A.; Julve, M.; Journaux, Y. *Inorg. Chem.* **1990**, *29*, 5054.

(12) (a) Berg, J. M.; Holm, R. H. In *Iron-Sulfer Proteins*; Spioro, T. G., Ed.; Wiley-Interscience: New York, 1982; Vol. 4, Chapter 1. (b) Holm, R. H.; Ciurli, S.; Weigel, J. A. *Prog. Inorg. Chem.* **1990**, *38*, 1.

(13) Yang, E.-C.; Wernsdorfer, W.; Hill, S.; Edward, R. S.; Nakano, M.; Maccagnano, S.; Zakharov, L. N.; Rheingold, A. L.; Christou, G.; Hendrickson, D. N. *Polyhedron* **2003**, *22*, 1727.

(14) Gatteschi, D.; Sorace, L. *J. Solid State Chem.* **2001**, *159*, 253.

(15) Oshio, H.; Hoshino, N.; Ito, T. *J. Am. Chem. Soc.* **2000**, *122*, 12602.

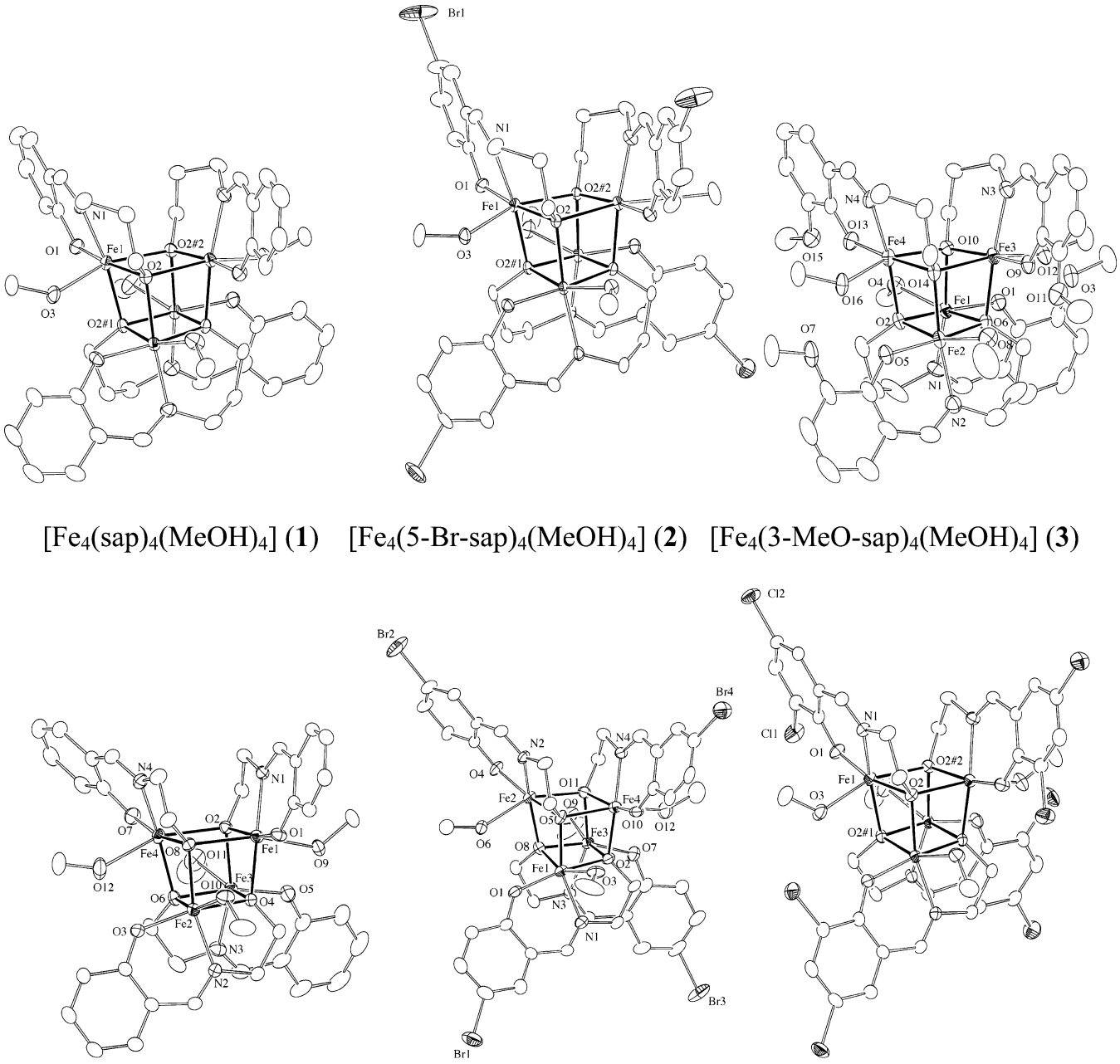

$[Fe_4(sap)_4(MeOH)_4]$ (**1**) $[Fe_4(5\text{-Br-sap})_4(MeOH)_4]$ (**2**) $[Fe_4(3\text{-MeO-sap})_4(MeOH)_4]$ (**3**)

$[Fe_4(sae)_4(MeOH)_4]$ (**4**) $[Fe_4(5\text{-Br-sae})_4(MeOH)_4]$ (**5**) $[Fe_4(3,5\text{-}Cl_2\text{-sae})_4(MeOH)_4]$ (**6**)

Figure 1. ORTEP diagrams of $[Fe_4(sap)_4(MeOH)_4]\cdot 2H_2O$ (**1**), $[Fe_4(5\text{-Br-sap})_4(MeOH)_4]$ (**2**), $[Fe_4(3\text{-MeO-sap})_4(MeOH)_4]\cdot 2MeOH$ (**3**), $[Fe_4(sae)_4(MeOH)_4]$ (**4**), $[Fe_4(5\text{-Br-sae})_4(MeOH)_4]\cdot 2MeOH$ (**5**), and $[Fe_4(3,5\text{-}Cl_2\text{-sae})_4(MeOH)_4]$ (**6**) with 30% probability.

Å, respectively. In **4**−**6**, the axial bond lengths are 2.282(2), 2.299(10), and 2.264(2) Å, and shorter equatorial bond lengths (1.9874(17)−2.0944(16), 1.9777(7)−2.083(8), and 1.9718(14)−2.0817(13) Å) are, respectively, observed. The different coordination environments are due to the steric strain on the Fe^{II} ions. The equatorial sites of each Fe^{II} ion in **1**−**3** are coordinated by two six-membered chelates, while those in **4**−**6** have six- and five-membered chelates. The octahedrons about the Fe^{II} ions in **4**−**6** are, therefore, more squeezed in the equatorial plane than those in **1**−**3**. The differences in the JT distortion modes lead to the different behaviors in ac magnetic susceptibility data. The bridging angles of the Fe−O−Fe bonds, which determine the sign of the magnetic exchange interactions through oxygen bridges, are in the ranges 93.95(5)°−101.76(6)°, 94.43(9)°−100.57(11)°, 94.16(17)°−101.15(17)°, and 93.06(6)°−103.61(7)°, 94.1(3)°−101.1(3)°, and 93.62(5)°−101.34(5)° for **1**−**6**, respectively.

Magnetic Properties. Magnetic susceptibility measurements (Figure 2a and 3a) for **1**−**6** were performed in the temperature range 1.8−300 K. The $\chi_m T$ values for each complex showed similar temperature profiles, and the values at 300 K are 15.42−16.41 emu mol^{-1} K, which are larger than the value (12.0 emu mol^{-1} K with $g = 2$) expected for an uncorrelated sum of four Fe(II) ions. The $\chi_m T$ values gradually increased as the temperature was lowered, and they reached a maximum value around 10 K, which was followed by sudden decrease. The behavior is characteristic of ferromagnetic interactions and indicates $S = 8$ spin ground states for **1**−**6**. Subtle differences in the

Table 1. Selected Bond Lengths [Å] for **1**−**3**[a]

	$[Fe_4(sap)_4(MeOH)_4]\cdot 2H_2O$ (**1**)		
Fe(1)−O(1)	2.0290(16)	Fe(1)−O(2)	2.0447(15)
Fe(1)−N(1)	2.127(2)	Fe(1)−O(2)#1	2.1616(15)
Fe(1)−O(3)	2.2107(17)	Fe(1)−O(2)#2	2.2505(14)
	$[Fe_4(5\text{-Br-sap})_4(MeOH)_4]$ (**2**)		
Fe(1)−O(1)	2.036(3)	Fe(1)−O(2)	2.056(3)
Fe(1)−N(1)	2.123(3)	Fe(1)−O(2)#1	2.159(3)
Fe(1)−O(2)#2	2.259(2)	Fe(1)−O(3)	2.263(3)
	$[Fe_4(3\text{-MeO-sap})_4(MeOH)_4]\cdot$ 2MeOH (**3**)		
Fe(1)−O(1)	1.991(5)	Fe(1)−O(2)	2.037(4)
Fe(1)−N(1)	2.104(6)	Fe(1)−O(10)	2.137(4)
Fe(1)−O(6)	2.238(4)	Fe(1)−O(4)	2.242(5)

[a] Key to symmetry operations: (#1) $-y + 5/4$, $x + 1/4$, $-z + 9/4$ and (#2) $-x + 1$, $-y + 3/2$ for **1**, and (#1) $y - 1/4$, $-x + 5/4$, $-z + 9/4$ and (#2) $-x + 1$, $-y + 3/2$, z for **2**.

Table 2. Selected Bond Lengths (Å) of **4**−**6**[a]

	$[Fe_4(sae)_4(MeOH)_4]$ (**4**)		
Fe(1)−O(1)	1.9784(17)	Fe(1)−N(1)	2.053(2)
Fe(1)−O(4)	2.0775(17)	Fe(1)−O(2)	2.0944(16)
Fe(1)−O(8)	2.2736(17)	Fe(1)−O(9)	2.2908(18)
	$[Fe_4(5\text{-Br-sae})_4(MeOH)_4]\cdot$2MeOH (**5**)		
Fe(1)−O(1)	1.977(7)	Fe(1)−O(5)	2.071(7)
Fe(1)−O(2)	2.077(6)	Fe(1)−N(1)	2.083(8)
Fe(1)−O(8)	2.273(7)	Fe(1)−O(3)	2.326(7)
	$[Fe_4(3,5\text{-}Cl_2\text{-sae})_4(MeOH)_4]$ (**6**)		
Fe(1)−O(1)	1.9718(14)	Fe(1)−N(1)	2.0654(17)
Fe(1)−O(2)#1	2.0808(13)	Fe(1)−O(2)	2.0817(13)
Fe(1)−O(2)#2	2.2480(13)	Fe(1)−O(3)	2.2799(17)

[a] Key to symmetry operations: (#1) $-y + 5/4$, $x - 3/4$, $-z + 9/4$ and (#2) $-x + 2$, $-y + 1/2$, z for **6**.

magnetic behaviors are due to the different amplitudes of g values, intramolecular exchange coupling constants (J), zero-filed splitting parameters (D), and intermolecular antiferromagnetic interactions. The magnetic susceptibility data above 20 K were analyzed using the Heisenberg spin Hamiltonian $H = -2J_1(S_1\cdot S_2 + S_1\cdot S_3 + S_2\cdot S_4 + S_3\cdot S_4) - 2J_2(S_1\cdot S_4 + S_2\cdot S_3)$, assuming a cubic arrangement with D_{2d} symmetry, and the J values for **1**−**6** were estimated to be in the range 0.6−1.0 cm^{-1}. More accurate J values can be obtained by including both antiferromagnetic intermolecular interactions and the ZFS terms. However the Curie and Weiss constants were calculated using the data above 50 K and listed in Table 3, and the estimated Curie constants 13.44−15.43 emu mol^{-1} K correspond to the g value range 2.12−2.26.

Plots of the magnetization data at 1.8 K as a function of applied magnetic field up to 5 T are shown in Figures 2b and 3b. The $M/N\mu_B$ values did not show saturation up to 5 T, and the magnetic field dependencies did not follow the Brillouin function for an $S = 8$ ground state. The M vs H/T data at 1.8 K were fitted on the assumption of only the ground state of $S = 8$ being populated. The spin Hamiltonian was constructed using the sum of the isotropic Zeeman and axial ZFS terms,[16] and the 17 × 17 (=$(2S + 1)^2$) matrix was diagonalized to yield magnetization curves using a powder average procedure.[17] Least squares calculations using the g values estimated from the Curie plots gave the positive and negative D values for **1**−**3** (+0.80 to +1.15 cm^{-1}) and **4**−**6** (−0.66 to −0.76 cm^{-1}), respectively. Although more reliable D values can be determined from high-field EPR (HF-EPR) measurements, the HF-EPR measurements (upto 350 GHz with 20 T) for single crystals showed only very broad signals at 4−50 K, possibly due to the rapid spin−spin relaxation.

Ac magnetic susceptibility measurements for polycrystalline samples were performed in the temperature range of 1.8−4.0 K with a 3 G ac field oscillating at 50−1000 Hz. Complexes **4**−**6** gave frequency-dependent in-phase (χ_m') and out-of-phase (χ_m'') signals, while the out-of-phase (χ_m'') signals for **1**−**3** were not observed down to 1.8 K. The ac magnetic susceptibility data for **5** and **6** are shown in Figures 4 and 5, respectively, and those for **4** have been already reported.[15] The χ_m' values for **4**−**6** increased as the temperature was lowered and reached a maximum value at 2.0−2.5 K which was followed by a decrease. The temperature dependency of the out-of-phase (χ_m'') signals showed peak maxima at 1.8−2.5 K which shifted to a lower temperature as the ac frequency decreased from 1000 to 50 Hz. The ac susceptibility data indicate that complexes **4**−**6** are SMMs. Assuming the relaxation time (τ) at the peak-top temperature is well approximated by the inverse of the ac frequency, Arrhenius plots of a relaxation time (τ) gave activation energies ΔE for spin reorientations ($M = 8$ to -8) at 28, 30, 26 K with pre-exponential factors (τ_0) of 3.63×10^{-9}, 1.89×10^{-9}, and 7.68×10^{-9} s, respectively (Figure 6). These τ_0 values are in the range of the values (10^{-8}−10^{-11} s) reported for superparamagnetic nanoparticles.[18] Magnetic hystereses for **4**−**6** were not observed at 1.8 K because of the cube's low blocking temperature (T_B = 1.1−1.2 K). It is noted that complexes **1**−**3** are non-SMM or have very low blocking temperature. But the latter can be ruled out because of the positive D values estimated by the magnetization experiments.

Discussions

Molecules with zero-field splitting of easy axis type ($D < 0$) have a double minimum potential in the revese direction of the magnetic moment with an energy barrier profile of $|D|S_z^2$. Molecules with negative D values and relatively high-spin ground states have slow magnetic relaxation of the spin flipping (from up to down spins) along the magnetic anisotropy axis at very low temperature. In the Fe^{II} cubes **1**−**6**, the alkoxo groups bridge four Fe^{II} ions with bond angles of 93°−104°. Thus, the magnetic orbitals are accidentally orthogonal, and the cubes have an $S = 8$ ground state. The spin Hamiltonian including magnetic anisotropy can be written as

$$H = g\mu_B HS + D[S_z^2 - S(S+1)/3] + E(S_x^2 - S_y^2)$$

where the first term represents the Zeeman energy, and the second and third terms are contributed from the magnetic anisotropies of uniaxial (D) and rhombic (E) zero field splittings. In **1**−**6**, the Fe^{II} ion has the tetragonal Jahn−Teller distortion, and the rhombic term is, therefore, presumed to be very small and can be ignored. The sign of the single ion D_{Fe} values depends on the electronic states of the Fe^{II} ion. In a high-spin Fe^{II} ion, tetragonal JT effects split the t_{2g} orbitals into the e_g and b_{2g} orbitals under D_{4h} symmetry, causing the ^5E_g or $^5B_{2g}$

(16) (a) Armoi, G.; Knapp, M. J.; Claude, J.-O.; Huffman, J. C.; Hendrickson, D. N.; Christou, G. *J. Am. Chem. Soc.* **1999**, *121*, 5489. (b) Eppley, H. J.; Tsai, H.-L.; de Vries, N.; Folting, K.; Christou, G.; Hendrickson, D. N. *J. Am. Chem. Soc.* **1995**, *117*, 301.
(17) Marath, V. R.; Mitra, S. *Chem. Phys. Lett.* **1974**, *27*, 103.
(18) Dormann, J. L.; Fiorani, D.; Tronc, E. *Advances in Chemistry Physics*; Prigoging, I., Rice, S. A., Eds.; John Wiley & Sons: 1997; Vol XCVIII.

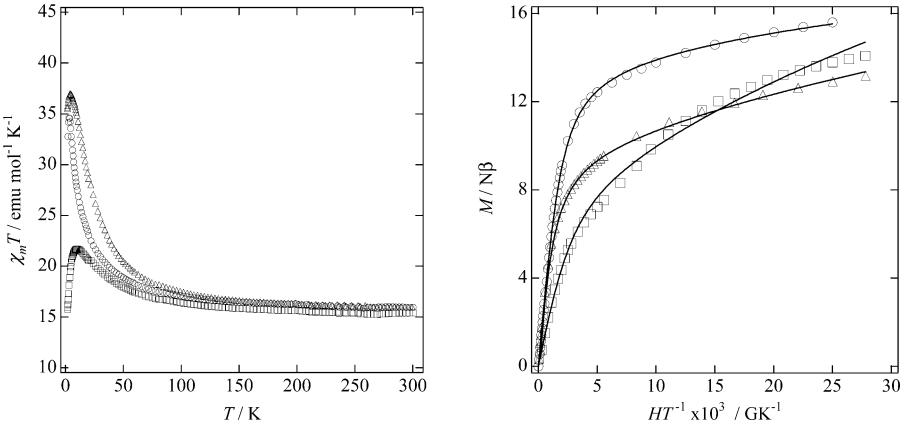

Figure 2. Plots of (a) $\chi_m T$ versus temperature and (b) M versus H/T for (○) $[Fe_4(sap)_4(MeOH)_4]\cdot 2H_2O$ (**1**), (□) $[Fe_4(5\text{-Br-sap})_4(MeOH)_4]$ (**2**), and (△) $[Fe_4(3\text{-MeO-sap})_4(MeOH)_4]\cdot 2MeOH$ (**3**). The solid line is the least-squares fit using the parameters described in the text.

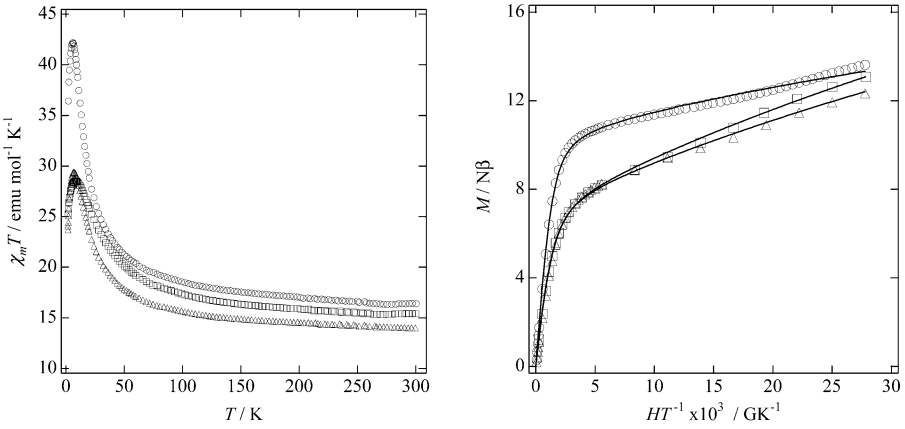

Figure 3. Plots of (a) $\chi_m T$ versus temperature and (b) M versus H/T for (○) $[Fe_4(sae)_4(MeOH)_4]$ (**4**), (□) $[Fe_4(5\text{-Br-sae})_4(MeOH)_4]\cdot 2MeOH$ (**5**), and (△) $[Fe_4(3,5\text{-}Cl_2\text{-sae})_4(MeOH)_4]$ (**6**). The solid line is the least-squares fit using the parameters described in the text.

Table 3. Summary of Magnetic Parameters Obtained from dc and Ac Magnetic Susceptibility Data

	g	c [emu mol^{-1} K]	θ [K]	D^a [cm^{-1}]	ΔE [K]	T_B [K]
$[Fe_4(sap)_4(MeO)_4]\cdot 2H_2O$ (**1**)	2.261	15.43	9.56	+0.8		
$[Fe_4(5\text{-Br-sap})_4(MeO)_4]$ (**2**)	2.227	14.86	9.32	+0.80		
$[Fe_4(3\text{-MeO-sap})_4(MeO)_4]\cdot 2MeOH$ (**3**)	2.243	15.27	12.59	+1.15		
$[Fe_4(sae)_4(MeO)_4]$ (**4**)	2.126	15.55	15.98	−0.76 (−0.31)	28	1.1
$[Fe_4(5\text{-Br-sae})_4(MeO)_4]\cdot MeOH$ (**5**)	2.209	14.57	15.68	−0.66 (−0.33)	30	1.2
$[Fe_4(3,5\text{-}Cl_2\text{-sae})_4(MeO)_4]$ (**6**)	2.120	13.44	13.99	−0.67 (−0.29)	26	1.1

[a] g, c, and θ values were obtained from the magnetic susceptibility data above 50 K. D values were estimated using magnetization data at 1.8 K with only the $S = 8$ ground state populated. D values in the parentheses, ΔE, and T_B values were estimated using the ac magnetic susceptibility data.

terms to become the ground state. The $^5B_{2g}$ and ^5E_g states do not have orbital angular momentum, but mixing with the other states by the spin−orbit coupling gives rise to magnetic anisotropies. The splitting of the t_{2g} (d_π) orbitals depends on both π-donating and accepting ability of the ligands, while π-back-donation in high-spin Fe^{II} ions is assumed to be small and can be ignored. It is considered that the d_{xz} and d_{yz} orbitals are destablized by π-donations from both axial and equatorial ligands; the b_{2g} orbital is, therefore, lower in energy than the e_g orbitals, and the $^5B_{2g}$ term becomes the ground state (Scheme 1).

Based on the ac magnetic susceptibility measurements, **4**−**6** are SMMs, and the analyses of magnetization data gave positive and negative D_{cube} values for **1**−**3** and **4**−**6**, respectively. From the X-ray structure analyses, the equatorial coordination bond lengths about the Fe^{II} ions in **4**−**6** are shorter than those for

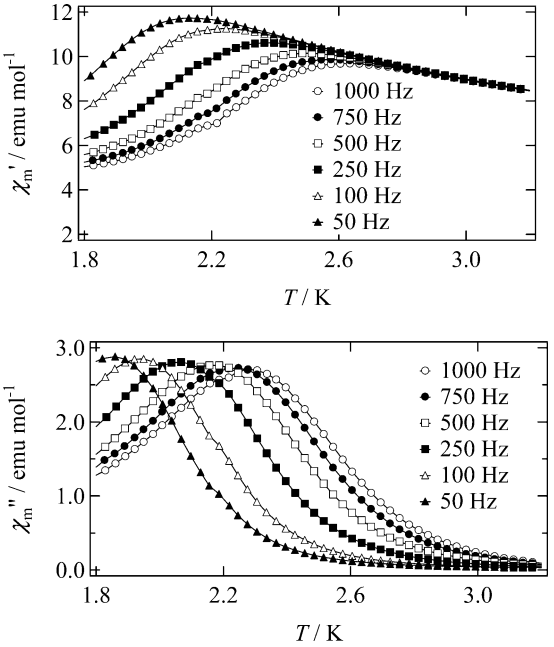

Figure 4. In-phase (χ_m') and out-of-phase (χ_m'') ac magnetic susceptibility versus temperature in a 3.0 G ac field oscillating at the indicated frequencies and with a zero dc field for $[Fe_4(5\text{-Br-sae})_4(MeOH)_4]\cdot 2MeOH$ (**5**).

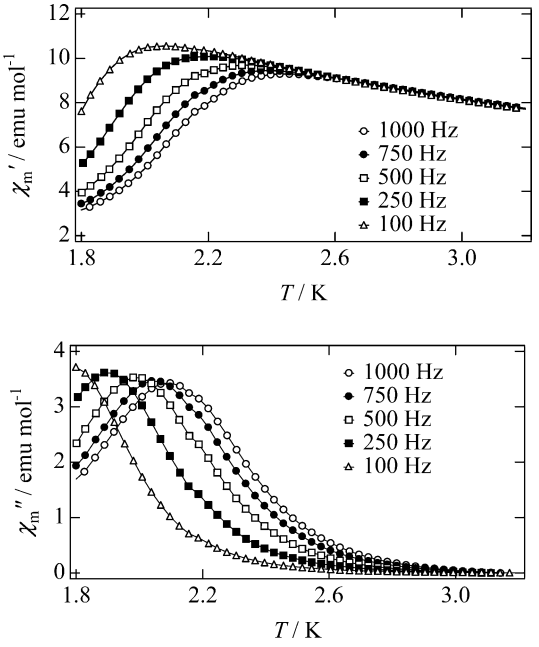

Figure 5. In-phase (χ_m') and out-of-phase (χ_m'') ac magnetic susceptibility versus temperature (T) in a 3.0 G ac field oscillating at the indicated frequencies and with a zero dc field for $[Fe_4(3,5\text{-}Cl_2\text{-sae})_4(MeOH)_4]$ (**6**).

1−**3**, meaning that the coordination spheres of the Fe^{II} ions in **4**−**6** are equatorially more compressed than those in **1**−**3** and that the π-donation from the equatorial sites to the Fe^{II} ions in **4**−**6** is stronger. The differences in JT distortions are responsible for the sign of the D_{Fe} values.

The energy splits of the $^5B_{2g}$ state of a single Fe^{II} ion were calculated using the angular overlap model (AOM).[19] Total Hamiltonian can be written as the sum of crystal field (H_{CF}), spin−orbit coupling (H_{LS}), electron repulsion (H_{ee}), and Zeeman (H_Z) terms as follows:[20]

$$H = H_{CF} + H_{LS} + H_{ee} + H_Z$$

$$H_{CF} = \sum_{i=1}^{N}[e_\sigma(i)\sum_{e_g}\sum_{e_g'}|e_g\rangle F_{eg}(\Omega_i)F_{eg'}(\Omega_i)\langle e_g'| + e_\pi^{\parallel}(i)\sum_{t_{2g}}\sum_{t_{2g}'}|t_{2g}\rangle F_{t_{2g}}^{\parallel}(\Omega_i)F_{t_{2g'}}^{\parallel}(\Omega_i)\langle t_{2g'}| + e_\pi^{\perp}(i)\sum_{t_{2g}}\sum_{t_{2g}'}|t_{2g}\rangle F_{t_{2g}}^{\perp}(\Omega_i)F_{t_{2g'}}^{\perp}(\Omega_i)\langle t_{2g'}|]$$

$$H_{LS} = k\sum_i \zeta \hat{l}_i \cdot \hat{s}_i$$

$$H_{ee} = \frac{1}{4\pi\epsilon_0}\sum_{i>j}\frac{e^2}{|r_i - r_j|}$$

$$H_Z = -\mu_B(k\hat{L} + \hat{S})\cdot B$$

N_L, $e_{\sigma \text{ or } \pi}(i)$, Ω_i, $F_{eg \text{ or } t_{2g}}$, k, and ζ represent coordination number, AOM parameter, Eulerian angle, overlap factor, Steven's orbital reduction factor, and spin−orbit coupling constant, respectively. Table 4 summarized the values of the ligand field strengths and the parameters used in the AOM calculations, which were taken from the references.[19] The elongated axis of the Fe^{II} ion involving the O(MeOH)−Fe−O(alkoxide) vector was used as the principal axis (*z*-axis) and the phenoxo O and imino N atoms make up the equatorial coordination sites forming the *x* and *y* axes, respectively. The

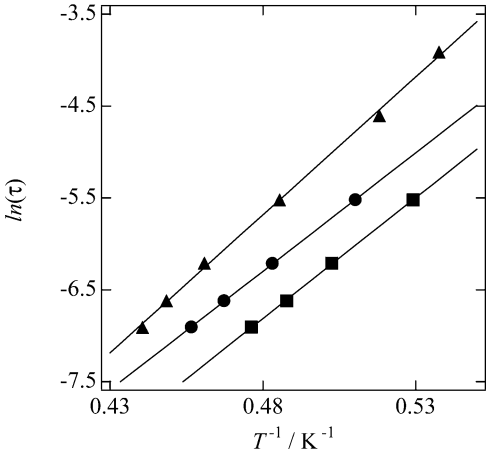

Figure 6. Plots of the ln(τ) versus the inverse of temperature (T^{-1}) for (●) $[Fe_4(sae)_4(MeOH)_4]$ (**4**), (■) $[Fe_4(5\text{-Br-sae})_4(MeOH)_4]\cdot 2MeOH$ (**5**), and (▲) $[Fe_4(3,5\text{-}Cl_2\text{-sae})_4(MeOH)_4]$ (**6**).

Scheme 1. d-Orbital Splitting Scheme under O_h and D_{4h} Point Groups

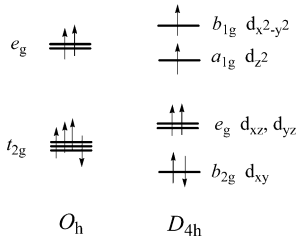

(19) (a) Figgis, B. N.; Hitchman, M. A. *Ligand Field Theory and Its Applications*; Wiley-VCH; 2000. (b) Schönherr, T. *Top. Curr. Chem.* **1997**, *191*, 88. (c) Hoggard, P. E. *Coord. Chem. Rev.* **1986**, *70*, 85. (d) Lever, A. B. P. *Inorganic Electronic Spectroscopy*, 2nd ed.; Elsevier: 1984. (e) Larsen, E.; La Mar, G. N. *J. Chem. Educ.* **1974**, *51*, 633.

(20) (a) Solomon, E. I.; Lever, A. B. P. *Inorganic Electronic Structure and Spectroscopy, Vol.1: Methodology*; John Wiley & Sons: 1999. (b) Schönherr, T. *Top. Curr. Chem.* **1997**, *191*, 88.

Table 4. Parameters Used in AOM (Angular Overlap Model) Calculations for Tetragonally Distorted Fe^{II} Centers[b]

	coordination atom	e_σ/hc cm^{-1}	$e_\pi(\|\|)^a/hc$ cm^{-1}	$e_\pi(\perp)^a/hc$ cm^{-1}
x-axis	O(phenoxy)	4800	1200	1200
	μ_3-O	4800	1200	1200
y-axis	N(imino)	3600	900*p*	0
	μ_3-O	4800	1200*p*	1200*p*
z-axis	O(MeOH)	2400	600	600
	μ_3-O	2400	600	600

[a] Ligand field strengths of parallel and perpendicular π-components to the *x*,*y*-plane. Racah parameters: $B/hc = 880.0$ cm^{-1} and $C/B = 3.75$. Spin−orbit coupling constant: $\zeta/hc = 412.0$ cm^{-1}. Steven's orbital reduction factor: $k = 0.8$. The variable *p* has the value of 0.5−1.0.[19] [b] *x* and *y* axes were taken as the vectors of Fe−O(phenoxo) and Fe−N(imine) bonds, respectively.

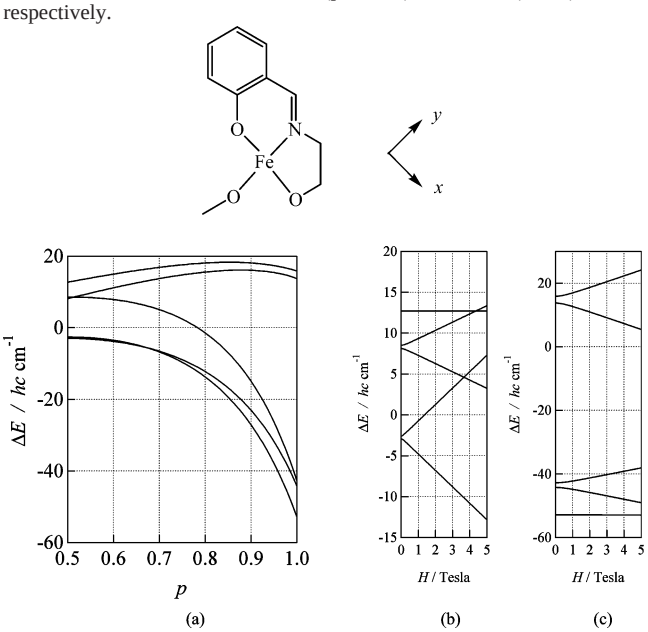

Figure 7. (a) Energy splitting scheme of the $^5B_{2g}$ state calculated for an octahedral $3d^6$ system subjected to N_1O_5 coordination. The variable *p* changes the ligand field strengths of $e_\pi(\|)$ and $e_\pi(\perp)$, and the parameters used in the calculations are listed in Table 4. Energy splitting schemes by the applied magnetic field parallel to the *y*-axis with (b) $p = 0.5$ and parallel to the *x*-axis with (c) $p = 1.0$.

σ- and π-donating ability of ligand donor sets are summarized as e_σ, parallel ($e_\pi(\|)$), and perpendicular ($e_\pi(\perp)$) components to the *xy*-plane, respectively. The ligand field strengths of the e_σ were fixed, while the strengths of $e_\pi(\|)$ and $e_\pi(\perp)$ were treated as the variables by introducing the parameter (*p*) (see Table 4). When the *p* value becomes less than the unity, the π-donation of the equatorial ligands becomes weak.

The calculated energy splitting scheme for a $3d^6$ system subjected to N_1O_5 coordination are shown in Figure 7a. If the π-donation from the equatorial ligands is weak ($p = 0.5$), the $^5B_{2g}$ term is not a good eigenstate and it splits into two nearly degenerate states and one nondegenerate state. Calculations with the magnetic field along the *y*-axis gave a quasi-first-order Zeeman effect involving the low-lying nearly degenerate states, suggesting that the split states, where the equatorial π-donation is weak, correspond to the $M_s = \pm 2$, ± 1, and 0 states in order from the lowest energy (Figure 7b). Therefore, the Fe^{II} ions in **1**−**3** have negative D_{Fe} values. When the equatorial π-donation is strong ($p = 1$), the $^5B_{2g}$ state was split into five states and the two sets of the higher energy states show Zeeman splits by the magnetic field along the *x*-axis (Figure 7c). The lowest state

Scheme 2. (a) Collinear Easy-Axis ($D_{Fe} < 0$) Alignment and (b) Orthogonal Hard-Axis ($D_{Fe} > 0$); Alignments Required for the Negative D_{cube} Value

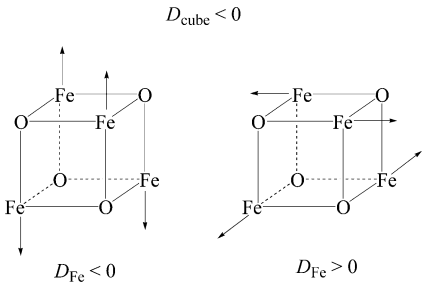

was assigned to the $M_s = 0$ state, which corresponds to the positive value of D_{Fe} for the Fe^{II} ion in **4**−**6**. It appears that the value of D_{Fe} changes its sign from the positive to negative as the equatorial π-donation becomes weaker.

It should be noted that from the AOM calculation the Fe^{II} ions in **4**−**6** have positive D_{Fe} values but the magnetic measurements gave the negative D_{cube} values for the cube. Structure analyses for the cubes showed that the four elongated axes are perpendicular to the molecular S_4 axis and that the two parallel elongated axes lying on the upper and lower faces of the cube are perpendicular to each other. The negative D_{cube} values are due to two possible origins based on the classical vector picture: the collinear and orthogonal alignments of four ions with easy axis ($D_{Fe} < 0$) and hard axis ($D_{Fe} > 0$) magnetic anisotropy, respectively (Scheme 2).[21] The latter explains the situations for **4**−**6**. However, in **1**−**3** the four Fe^{II} ions with negative D_{Fe} values are aligned in such a way to give positive D_{cube} values.

Conclusion

A new series of SMMs has been successfully prepared and studied. Dc magnetic susceptibility measurements showed that the Fe^{II} ions in the cubes are ferromagnetically coupled and the cubes have an $S = 8$ spin ground state. Analyses of magnetization experiments gave positive values of D_{cube} for **1**−**3** and negative values for **4**−**6**, and variable temperature ac susceptibility measurements down to 1.8 K showed peak maxima of out-of-phase signals for the latter. The Fe^{II} ions in the cubes have tetragonal Jahn−Teller distortions, with the Fe^{II} ions in **4**−**6** having shorter coordination bond lengths at the equatorial positions. AOM calculations gave positive D_{Fe} values for the Fe^{II} ions in **4**−**6**, and the perpendicular orientation of the single-ion D_{Fe} tensors resulted in an easy axis magnetic anisotropy for the entire cubes.

Experimental Section

Synthetic Procedures. All reagents were obtained from commercial suppliers and were used without further purification. All solvents were degassed by purging nitrogen prior to use. All syntheses and sampling for SQUID measurements were performed under an atmosphere of nitrogen using Schlenk techniques and a drybox unless otherwise noted.

$[Fe_4(sap)_4(MeOH)_4]\cdot 2H_2O$ (1). Salicylaldehyde (122 mg, 1 mmol), 3-amino-1-propanol (75 mg, 1 mmol), and triethylamine (202 mg, 2 mmol) were dissolved in methanol (10 mL), forming a yellow solution. To this solution was added $FeCl_2\cdot 4H_2O$ (198 mg, 1 mmol) in 10 mL of methanol. A dark brown solution occurred which was allowed to

(21) Nakano, M.; Matsubayashi, G.; Muramatsu, T.; Kobayashi, T.; Amaya, K.; Yoo, J.; Christou, G.; Hendrickson, D. N. *Mol. Cryst. Liq. Cryst.* **2002**, *376*, 405.

stand for a week, and dark blue tablets of **1** were obtained. Yield (35%). Anal. Calcd for $C_{44}H_{64}Fe_4N_4O_{14}$: C, 48.20; H, 5.88; N, 5.11. Found: C, 48.32; H, 5.74; N, 5.33.

[Fe_4(5-Br-sap)$_4$(MeOH)$_4$] (2). In a manner similar to that for **1**, 5-bromosalicylaldehyde (201 mg, 1 mmol), 3-amino-1-propanol (75 mg, 1 mmol), triethylamine (202 mg, 2 mmol), and $FeCl_2 \cdot 4H_2O$ (198 mg, 1 mmol) gave **2**. A dark brown solution occurred which was allowed to stand for a week, and dark blue tablets of **2** were obtained. Yield (33%). Anal. Calcd for $C_{44}H_{56}Br_4Fe_4N_4O_{12}$: C, 38.41; H, 4.10; N, 4.07. Found: C, 38.93; H, 3.84; N, 4.28.

[Fe_4(3-MeO-sap)$_4$(MeOH)$_4$]·2MeOH (3). In a manner similar to that for **1**, 3-methoxysalicylaldehyde (191 mg, 1 mmol), 3-amino-1-propanol (75 mg, 1 mmol), triethylamine (202 mg, 2 mmol), and $FeCl_2 \cdot 4H_2O$ (198 mg, 1 mmol) gave **3**. A dark brown solution occurred which was allowed to stand for a week, and dark blue tablets of **3** were obtained. Yield (33%). Anal. Calcd for $C_{50}H_{76}Fe_4N_4O_{18}$: C, 48.25; H, 6.16; N, 4.50. Found: C, 48.36; H, 6.41; N, 4.63.

[Fe_4(sae)$_4$(MeOH)$_4$] (4). In a manner similar to that for **1**, salicylaldehyde (122 mg, 1 mmol), 2-aminoethanol (61 mg, 1 mmol), triethylamine (202 mg, 2 mmol), and $FeCl_2 \cdot 4H_2O$ (198 mg, 1 mmol) gave **4**. A dark brown solution occurred which was allowed to stand for a week, and dark blue tablets of **4** were obtained. Yield (35%). Anal. Calcd for $C_{40}H_{52}Fe_4N_4O_{12}$: C, 47.84; H, 5.22; N, 5.58. Found: C, 47.66; H, 5.47; N, 5.83.

[Fe_4(5-Br-sae)$_4$(MeOH)$_4$]·MeOH (5). In a manner similar to that for **1**, 5-bromosalicylaldehyde (122 mg, 1 mmol), 2-aminoethanol (61 mg, 1 mmol), triethylamine (202 mg, 2 mmol), and $FeCl_2 \cdot 4H_2O$ (198 mg, 1 mmol) gave **5**. A dark brown solution occurred which was allowed to stand for a week, and dark blue tablets of **5** were obtained. Yield (30%). Anal. Calcd for $C_{41}H_{52}Br_4Fe_4N_4O_{13}$: C, 36.43; H, 3.88; N, 4.14. Found: C, 36.76; H, 3.72; N, 4.23.

[Fe_4(3,5-Cl_2-sae)$_4$(MeOH)$_4$] (6). In a manner similar to that for **1**, 3,5-dichlorosalicylaldehyde (122 mg, 1 mmol), 2-aminoethanol (61 mg, 1 mmol), $NaOCH_3$ (108 mg, 2 mmol), and $FeCl_2 \cdot 4H_2O$ (198 mg, 1 mmol) gave **6**. A dark brown solution occurred which was allowed to stand for a week, and dark blue tablets of **6** were obtained. Yield (30%). Anal. Calcd for $C_{40}H_{44}Cl_8Fe_4N_4O_{12}$: C, 37.54; H, 3.47; N, 4.38. Found: C, 37.85; H, 3.61; N, 4.71.

Physical Measurement. Magnetic susceptibility data were collected in the temperature range of 1.8 to 300 K and in an applied field of 10 kG of a Quantum Design model MPMS SQUID magnetometer. Pascal's constants were used to determine the diamagnetic corrections.[22]

X-ray Data Collection and Structure Refinement. Single crystals of **1** ($0.2 \times 0.25 \times 0.4$ mm^3), **2** ($0.30 \times 0.32 \times 0.44$ mm^3), **3** ($0.30 \times 0.35 \times 0.35$ mm^3), **4** ($0.25 \times 0.30 \times 0.35$ mm^3), **5** ($0.20 \times 0.20 \times 0.30$ mm^3), and **6** ($0.25 \times 0.25 \times 0.38$ mm^3) were mounted with epoxy resin on the tip of a glass fiber. Diffraction data were collected at −70 °C on a Bruker SMART 1000 diffractometer fitted with a CCD-type area detector, and a full sphere of data was collected by using graphite-monochromated Mo Kα radiation ($\lambda = 0.710\,73$ Å). At the end of data collection, the first 50 frames of data were recollected to establish that the crystal had not deteriorated during the data collection. The data frames were integrated using SAINT and were merged to give a unique data set for the structure determination. Empirical absorption corrections by SADABS (G. M. Sheldrick, 1994) were carried out, and relative transmissions are 1.000/0.843, 1.000/0.844, 1.000/0.895, 1.000/0.872, 1.000/0.832, and 1.000/0.927 for **1**−**6**, respectively. Totals of 19 811 ($1.7° < \theta < 26.1°$), 18 123 ($1.63° < \theta < 27.0°$), 20 532 ($1.4° < \theta < 26.1°$), 18 347 ($1.4° < \theta < 26.1°$), 28 661 ($1.0° < \theta < 24.11°$), and 19 203 ($1.64° < \theta < 28.0°$) reflections were, respectively, collected for **1**−**6**, which yielded 2427 ($R_{int} = 0.0289$), 2940 ($R_{int} = 0.0314$), 12663 ($R_{int} = 0.0434$), 8707 ($R_{int} = 0.0189$), 15 947 ($R_{int} = 0.1104$), and 3099 ($R_{int} = 0.0467$) independent reflections, respectively. Crystallographic data and structure refinement data are summarized in the Supporting Information. The structures were solved by direct methods and refined by the full-matrix least-squares method on all F^2 data using the SHELXTL 5.1 package (Bruker Analytical X-ray Systems). Non-hydrogen atoms were refined with anisotropic thermal parameters. Hydrogen atoms were included in calculated positions and refined with isotropic thermal parameters riding on those of the parent atoms. Full matrix least-squares refinements on F^2 converged to $R1/wR2$ ($I > 2\sigma(I)$) of 0.032/0.085, 0.061/0.167, 0.081/0.253, 0.034/0.090, 0.064/0.138, and 0.030/0.059 for **1**−**6**, respectively.

Acknowledgment. This work was partially supported by a Grant-in-Aid for Scientific Research from the Ministry of Education, Science, Sports and Culture, Japan, and by the COE and TARA projects in University of Tsukuba.

Supporting Information Available: X-ray structural information for **1**−**6**. Crystallographic details (CIF). This material is available free of charge via the Internet at http://pubs.acs.org.

JA0487933

(22) Hatfield, W. E. In *Theory and Application of Molecular Paramagnetism*; Boudreaux, E. A., Mulay, L. N., Eds.; Wiley and Sons: New York, 1976; pp 491−495.